Modeling and Simulation of a Massively Parallelized Multiphoton Polymerization 3D Microfabrication Process

Florie Ogor, Thomas Le Deun, Emma van Elslande, Azeddine Tellal, Akos Banyasz, Manuel Flury, Kevin Heggarty

Modelling and simulation of a massively parallelised multi-photon polymerization 3D microfabrication process

Florie Ogor Thomas Le Deun Emma Van Elslande Azeddine Tellal Akos Banyasz Manuel Flury Kevin Heggarty*

F. Ogor, Dr. T. Le Deun, Prof. K. Heggarty
IMT-Atlantique, Optics Department, Technopole Brest-Iroise, 29285 Brest, France
Email Address : florie.ogor@imt-atlantique.fr
E. Van Elslande, Dr. A. Tellal, Dr. A. Banyasz
Univ. Lyon, ENS Lyon, CNRS, Université Lyon 1, Laboratoire de Chimie, UMR 5182, 46 Allée d'italie, 69384 Lyon, France
Dr. M. Flury
ICube, Université de Strasbourg, CNRS, INSA, Strasbourg F-67000, France

Keywords: *Parallel microfabrication, 3D structures, scalar light propagation model, simulation*

While additive manufacturing based on multi photon polymerization is currently considered to be a very promising technique for the fabrication of 3D micro and nano structures, long fabrication times are a major limitation of this approach. Parallelization of the fabrication process is an important technique to overcome this issue. The fabrication process is parallelized by imaging a 1920x1080 pixel Spatial Light Modulator (SLM) into an ultra-sensitive Triplet-Triplet Annihilation (TTA) resist. However, proximity effects between close pixels generate uncontrolled polymerization and make the controlled fabrication of 3D structures difficult. This work models light propagation and chemical interactions in our system to predict fabricated structures with a view to precompensating plot data and improving 3D resolution by performing optical and chemical proximity correction. Our simple model gives reasonable predictions of fabricated structures helping us fabricate fully 3D structures in parallel.

1 Introduction

Multi-photon lithography is now widely recognised as a highly effective approach for the fabrication of high resolution (sub-micron) 3D structures that are required in a very wide range of applications: [1][2] from photonic devices to tissue engineering. [3] Micro-optics for sensors, [4]-[5] 3D bioscaffolds for in vitro study of cells or tissue engineering [6]-[7]-[8] are examples of structures that can be built by multi photon polymerization. To fabricate complex and highly-resolved 3D microstructures, a short pulse laser beam is usually focused in the resist using a high numerical aperture microscope objective. Currently, the main drawback of the technique is the slow write speed, inherent in the sub-micron voxel size, that limits industrial applications. Using galvo scanning mirrors is the fastest way to move the laser beam with respect to the sample (around 100 mm/s). [1] However, galvo scanning has a limited range of 2D motion. To create large 3D structures the galvo scanning is coupled with a three-axis stage, but the coordination can be complicated in terms of timing and position. The fundamental problem is the sequential single beam writing process. Numerous successful attempts have been made to parallelise the laser writing process using diffractive optical elements (DOE) [9]-[10]-[11] and microlens arrays [12] but the fixed nature of these optical elements limits fabrication to periodic structures. Phase Spatial Light Modulators (SLMs) have been used as reconfigurable DOEs to overcome this problem but low frame rates, DOE calculation time and DOE coding limit parallelisation factors and plot rates. In the case of 2D printing based on conventional one-photon photoplotting, a similar problem has been more or less solved by imaging amplitude SLMs using millions of write spots at 60 Hz framerates for multiphase LCD [13] or up to 1 kHz framerates for binary image Digital Mirrors Display (DMD). [14] Such approaches are difficult to use in multi-photon lithography because conventional resist sensitivity is too low to use full SLM pixel counts without exceeding SLM maximum admissible light power. Generally, to induce a quadratic nonlinearity versus light intensity, 3D nanoprinting methods rely, at the moment, on two-photon absorption and costly ultrafast lasers with peak intensities of order $10^{12} W/cm^2$. Recently alternative techniques such as upconversion luminescence, two step absorption and triplet-triplet annihilation have gained considerable interest [15]. These recent techniques also induce a quadratic nonlinearity versus intensity that make them suitable for 3D nanofabrication without requiring such expensive ultrafast lasers. In our parallel-write system, we use a conventional (low cost) amplitude

SLM in an imaging setup combined with a relatively low-cost continuous wave (CW) laser at a wavelength of 528 nm and a resist based on Triplet-Triplet Annihilation (TTA) [16]-[17]-[18]-[19] polymerization which has demonstrated submicron resolution with a comparatively low light intensity ($\approx 10\ W/cm^2$) continuous visible LED light source. However, we have discovered that when using multiple closely spaced write beams (here the pixels of the SLM) light overlap in "out-of-focus" planes produces undesired polymerisation and deforms fabricated structures resulting in a loss of 3D resolution. Temporal focussing techniques [20] and light sheet 3D microprinting [21] via two-colour two-step absorption can be used to overcome such problems but are complex and expensive. In this work we have attempted to model light propagation and chemical interactions to predict fabricated structures with a view to precompensating plot data and improving 3D resolution by performing optical and chemical proximity correction. Our digital simulation model uses a phenomenological approach to the photo-chemical process based on 3D optical propagation and chemical diffusion.

2 Simulation method

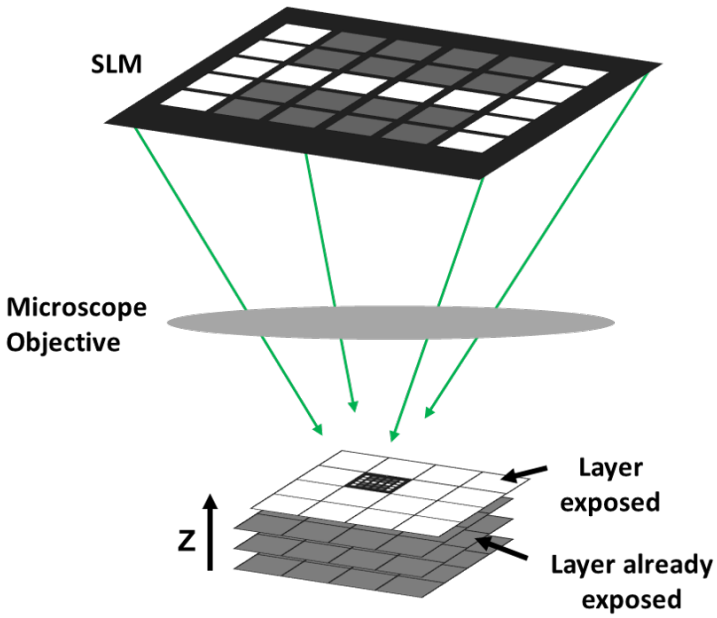

Figure 1: Schematic of our imaged SLM photoplotter : SLM imaged in the resist by a microscope objective

A schematic of our imaged SLM photoplotter and the flow diagram for our Matlab simulation of the parallel write fabrication process are shown in Figure 1 and Figure 2. After defining a 3D matrix corresponding to the sample volume, the approach can be divided into five main steps. We first propagate the light through the sample using a scalar light propagation model. Then to model the limited optical resolution of our system the light distribution is convolved with a 3D Gaussian function. The light distribution obtained is projected into the glass substrate and resist system. The Z position of the projection corresponds to the choice of the focus plane: fully in the resist or across the glass-resist interface. A second 3D Gaussian convolution is then performed to model the chemical diffusion processes of radicals, inhibitors, heat... that occur inside the resist. The final step is to polymerize, which is modeled by a thresholding, every voxel above the threshold is considered to be polymerized. The choice of the standard deviation of the two 3D Gaussians and of the polymerization threshold is empirical. These parameters are adjusted to best correspond to experimentally observed structures and conditions.

2.1 Scalar light propagation model

To model the propagation of light through the sample, a scalar light propagation method is used and more precisely a Fresnel Transfer Function propagator. [22] A vectorial light propagation method would give

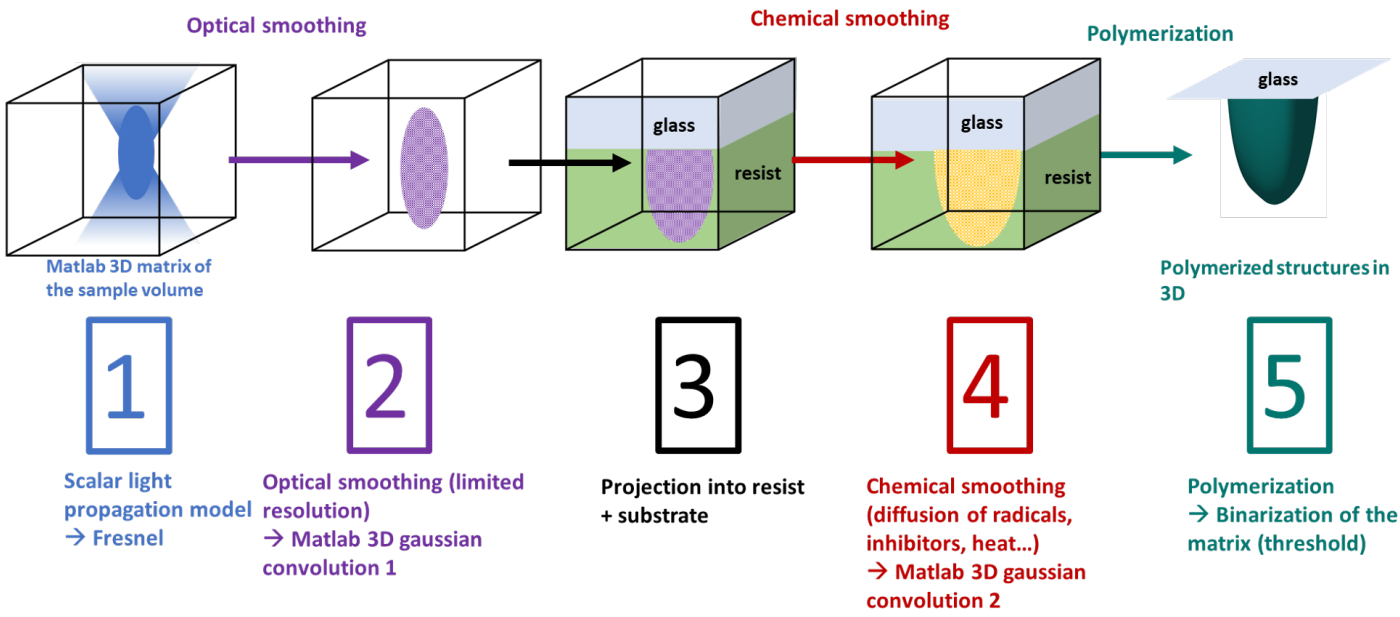

Figure 2: Flow diagram of our Matlab simulation

more accurate results but calculation times would be unfeasible for our application (volume 400x200x100 µm on 200 nm grid) and scalar propagation has proved sufficiently accurate in this initial approach. The propagation routine that we use is defined as follows :[22]

$$U_2(x,y) = \mathcal{F}^{-1}\left\{\mathcal{F}\left\{U_1(x,y)\right\} H(f_x,f_y)\right\} \tag{1}$$

with U_1 the source field, U_2 the observation field and H the transfer function given by :

$$H(f_x,f_y) = e^{j\frac{2\pi}{\lambda}z} exp\left[-j\pi\lambda z(f_x^2+f_y^2)\right] \tag{2}$$

with z the spatial propagation distance, λ the wavelength of the source, (x,y) the sample coordinates and (f_x,f_y) the frequency coordinates. We have chosen this propagator because it is suitable for short distance propagation ($z < \frac{L\Delta x}{\lambda}$ with L the array side length and Δx the sample interval) [22] corresponding to the tens of microns of resist that interests us here.

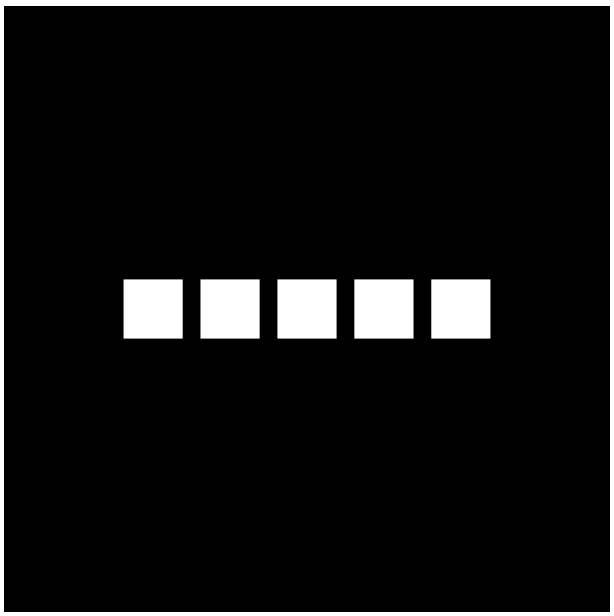

Figure 3: Amplitude of the input image of the scalar light propagation model

The amplitude of the source field U_1 used in the simulations was the same image file sent to the SLM in the experimental system (see Figure 3 for an example). The phase of the source field is also an important factor when simulating light propagation. Different phase functions were tested to simulate the fibre homogenised CW laser source used in our experimental system and a random phase found to give results closest to the experimental observations (see section 3.1 "3D Light distribution measurement").

To validate the implementation of the propagation routine, we checked that energy is conserved in the different Z planes and that we are in the validity domain of the model : short distance propagation. We also reproduced the self-imaging Talbot effect [23] for periodic objects in the expected planes ($Z_T = 2m\frac{d^2}{\lambda}$ with m a positive integer, d the object period).

2.2 Limited optical resolution of the system

A frequently used technique for modelling the limited optical resolution of image projection systems [24] is to perform spatial frequency filtering based on the illumination wavelength, refractive index in the object space and projection objective numerical aperture. [25] Here, given that our optical path contains many optical components (tube lenses, microscope objective, cubes...), it is difficult to model the optical resolution analytically. Instead, we chose to model the limited-resolution of our system (including the objective NA) by convolving the projected light distribution by a 3D Gaussian function. The width of the 3D gaussian function was determined empirically to give the best fit to the experimental observations (see section 3.1). Modelling of microscope objective 3D point spread functions (for example using PSF Generator [26]) would suggest that the use of 3D gaussian functions with different widths in the lateral (X,Y) and axial (Z) directions would be more accurate than a simpler gaussian function with equal widths in lateral and axial dimensions. In fact we found that there was no improvement in the match to experimental observations when using more complex 3D gaussian functions so (for our Zeiss Plan-aprochromat X40, NA 0.95 objective) a gaussian function standard deviation of 184 nm both in lateral (X,Y) and axial (Z) directions was used. We suspect that this is because our approach models the propagation of light along the optical axis so the increased extent of the projected light distribution in this direction is already taken into account. Optimizing the standard deviation of the 3D Gaussian function could be an interesting direction for future improvements.

2.3 Projection into resist and glass system

The light distribution obtained is then projected into the glass and resist system as shown in Figure 4. When making structures, it is possible to focus more or less deeply in the resist depending on the structure we wish to fabricate. The choice of focus plane is especially important for the fabriation of fully 3D structures that require multiple exposures in different focus planes. Furthermore, the positioning of the focus plane relative to the interface determines the stability of the obtained 3D microstructures.

2.4 Diffusion of chemical species and heat in the resist

The resist used is based on a Triplet-Triplet Annihilation process. In such a resist, the incident light is absorbed by a triplet photosensitizer, that undergoes intersystem crossing to generate triplet states. Upon interaction of the excited photosensitizer with a so-called annihilator it populates the triplet excited state of this second one via triplet-triplet energy transfer. Once the population of the annihilator in the triplet state is high enough, two excited annihilators may encounter and undergo triplet-triplet annihilation resulting in a ground state annihilator and an annihilator in a singlet excited state, which can then activate a photoinitiator. The resolution of TTA polymerization is expected to be determined by the combination of the size of the excitation volume and diffusional broadening of the various excited-state species that depends on several parameters such as the viscosity of the used photoresist and mobility of the various species such as molecules in triplet excited state, radicals and inhibitors.[15] - [18] Heat during photopolymerization originates from different phenomena: accumulated and then dissipated energy from one photon or multi-photon absorption and exothermic reactions. [11] We model the diffusion of reactive species and heat by

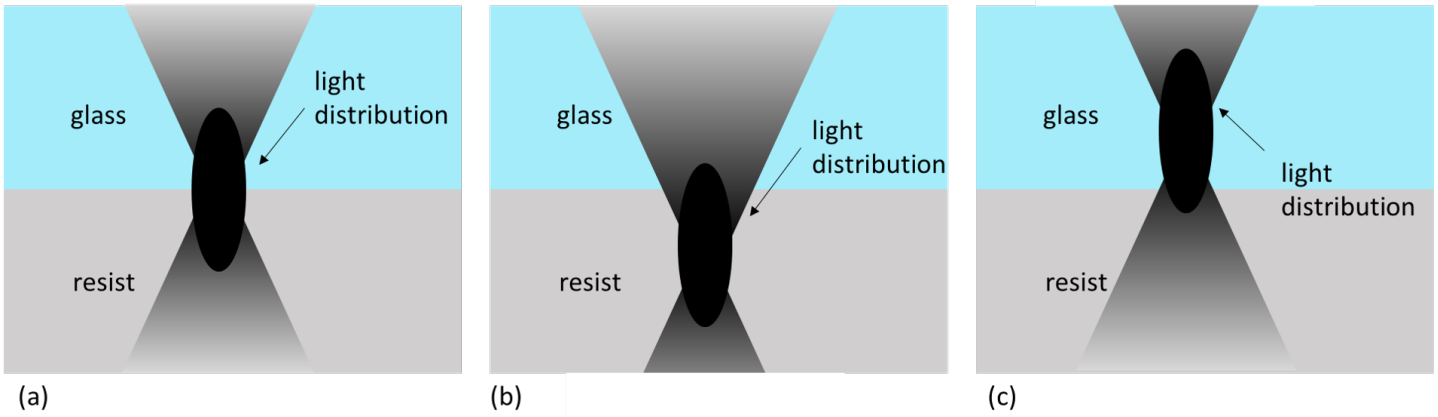

Figure 4: Projection into resist and glass system (a) focus at the interface (b) focus below the inferface (c) focus above the interface

a second convolution with a 3D Gaussian function that we call a chemical smoothing. Best agreement with experimental observations was obtained with a chemical smoothing 3D Gaussian function standard deviation of 2.1 µm. This is significantly larger than the optical smoothing function standard deviation (section 2.2) which suggests that in the case of our TTA resist, diffusion of chemical species appears to be the major factor limiting resolution. Studying TTA resists remains attractive however because of their very high sensitivity : of the order $10W/cm^2$. [15]

2.5 Polymerization

As TTA is a complex process involving a number of photoactive species, its kinetics are particularly challenging to model. [27] Yet, TTA-based resins retain a non-linear response that can be conveniently approximated by a simpler two-photon absoprtion-like behaviour, in which the excitation density has a quadratic dependance to light intensity. [1] Our simple model assumes that the 3D distribution of active species generated in the resist after the light absorption is proportional to the square of the light intensity distribution in the focal volume. We then assume that the resist is polymerized in resist volumes where the concentration of active species is sufficiently high, i.e. greater than an empricially determined threshold value. This is of course a very simplistic model for what is certainly a far more complex process but, as shown below, it nevertheless seems to give a reasonable fit to the experimentally observed structures. Our digital simulations therefore take the square of the simulated 3D light intensity distribution obtained after the "optical smoothing" convolution to obtain a 3D distribution of active species. We then apply the "chemical smoothing" 3D convolution to this 3D distribution of active species to allow for chemical diffusion effects. Finally we apply a threshold to the resulting 3D distribution to model polymerization : every voxel of the 3D matrix above the threshold is considered to be polymerized. In this way, we obtain the final shape of the fabricated structure. As before we adopt a phenomenological approach by adapting our simulation parameters (standard deviation of the chemical smoothing and the polymerisation threshold) to obtain results as close as possible to fabricated structures.

3 Experimental results

3.1 3D light distribution measurement

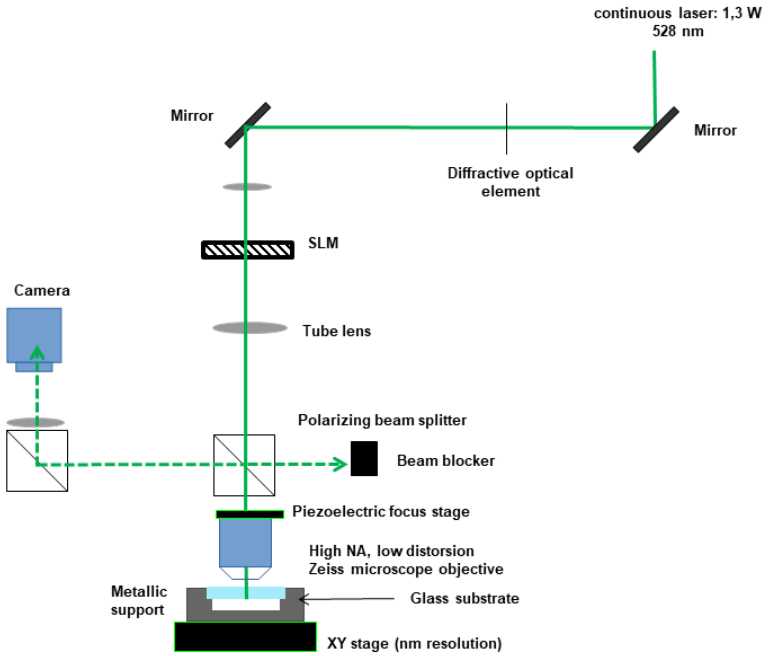

Figure 5: Schematic of our imaged SLM photoplotter : SLM imaged in the resist by a microscope objective

To check that our light distribution model was sufficiently close to the true situation in our experiments, we acquired a Z-stack of 2D light distributions. To obtain each Z-stack image, a pattern displayed on the SLM was imaged onto a glass substrate in the sample plane as shown in Figure 5. For example, here the image displayed on the SLM and in the input of the simulation consists of five white squares of side 21.25 µm on a black background (Figure 3). By scanning the substrate in the Z direction and capturing the light pattern reflected by the substrate on the observation camera for different positions of the substrate along the optical axis a Z-stack of images was obtained. The substrate was scanned along the Z-axis over a distance of 100 µm with a step of 1 µm to obtain a stack of 100 images. Patterns shown in Figure 6 (a) and (b) were obtained by taking a sectional view of the recorded Z-stack of images and of the simulated light diffraction pattern. To better compare simulations and experimental records, the step between two images of Z-piles was 1 µm for both light distributions. By comparing views in the XZ plane of the simulations and the light recordings, the standard deviation of the 3D Gaussian fucntion used to simulate the limited resolution of the optical system was adjusted to best match the simulations and the light recordings. The experimental data of Figure 6 b) seem to indicate the presence of spherical aberrations in the optical system. However this may result from the way light patterns are capturated by the optical system shown in Figure 5. The light captured by the system observation camera passes through the microscope objective and polarising beam splitter twice and there is an additional lens before the camera. These elements could induce spherical aberrations in the captured images that are not necessarily present in the projected patterns as the microscope objective used is corrected for the spherical aberration introduced by focussing though the substrate (here a standard thickness microscope coverslip). Placing the camera in the object plane to directly measure the experimental projected light pattern is not a feasible solution as the available cameras do not have sufficient resolution to correctly capture the focal plane pattern. The interface between glass and resist could probably be modeled more accurately by the scaled defocus model [28]. At this stage,

however we consider that simulations and light records shown in Figure 6 are close enough for our present needs.

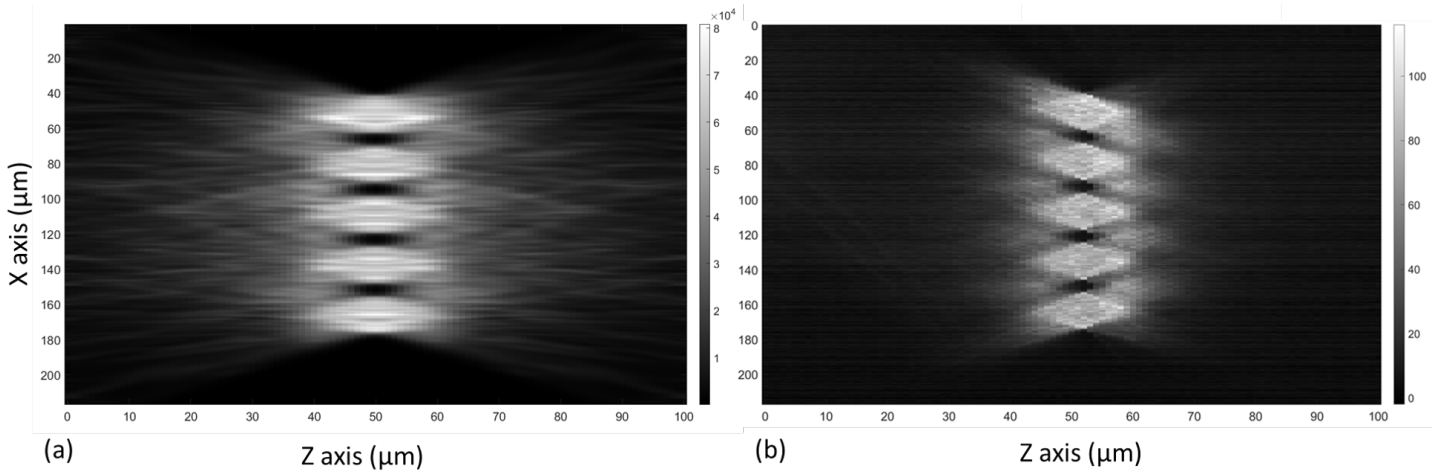

Figure 6: Sectional view of the Z-stack in the plane XZ. (a) simulated light distribution (b) Experimentally measured light distribution

3.2 Fabricated structures

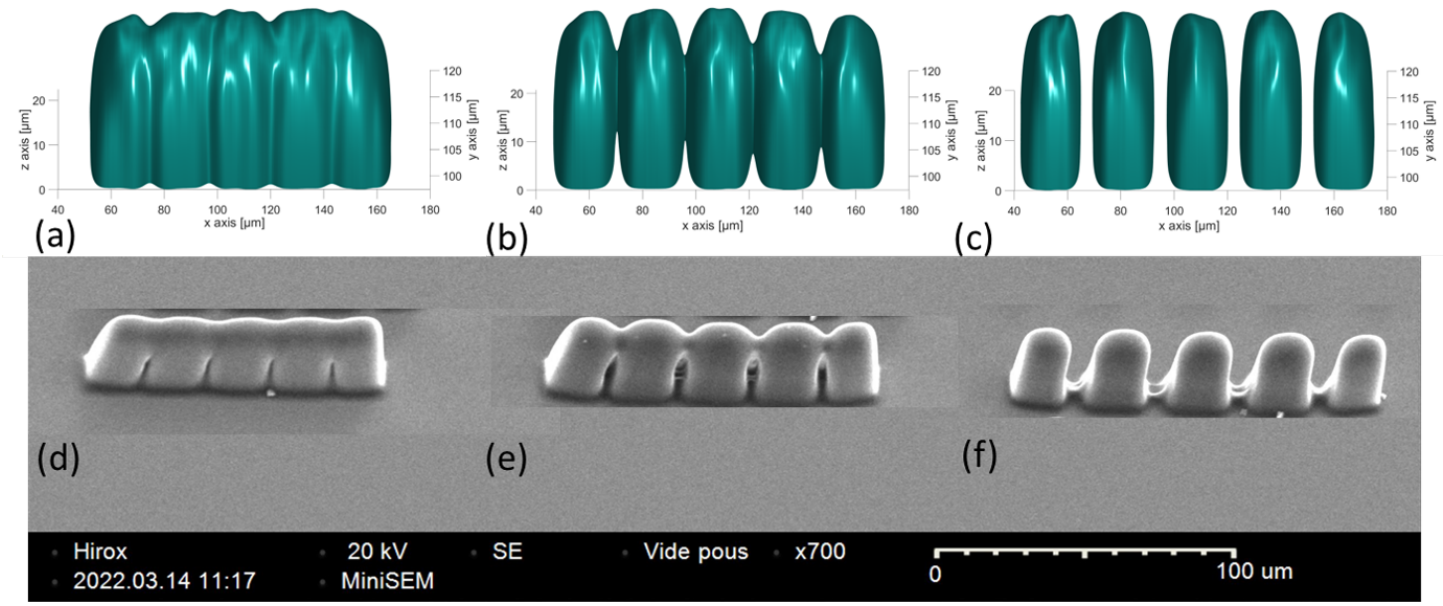

Figure 7: 3D view of simulated structures (a) cubes separated by 1.5 µm (b) cubes separated by 4.25 µm (c) cubes separated by 6.4 µm. Scanning electron microscope images of cubes separated by (d) 1.5 µm (e) 4.25 µm (f) 6.4 µm distances.

The last step was to ensure that the simulated structures were sufficiently close to structures fabricated in our experiments by selecting appropriate threshold values. In our simulations the light intensity distribution values are entirely arbitrary and not calibrated to experimental values (extracting reliable physical information from complex resists such as those based on the TTA process is notoriously difficult). [27] Hence unlike the Gaussian distribution standard deviation widths which can be linked to physical parameters through the simulation spatial sampling voxel dimensions, it is very difficult to give a physically meaningful quantification to the simulation threshold values. Threshold values relative to the simulated peak or average reactive species density are more useful in practice. Typical simulation thresholds used were close to 30% of the peak simulated reactive species density. With such thresholds the simulations

closely resemble the observed structures, as depicted in Figure 7. When the spacing between cubes is equal to 1.5 µm, they fuse and we obtain a single block (Figure 7 a and d). When cubes are separated by 4.25 µm, bridges start to appear because of overlapping in out-of-focus planes (7 b and e). When cubes are completely separate, we obtain separate pillars in the simulation as shown in Figure 7 c and f. Despite their simplicity, our simulations seem to corectly describe the general tendencies of the structures during the microfabrication with projection system using a TTA resin.

3.2.1 Fully 3D structures

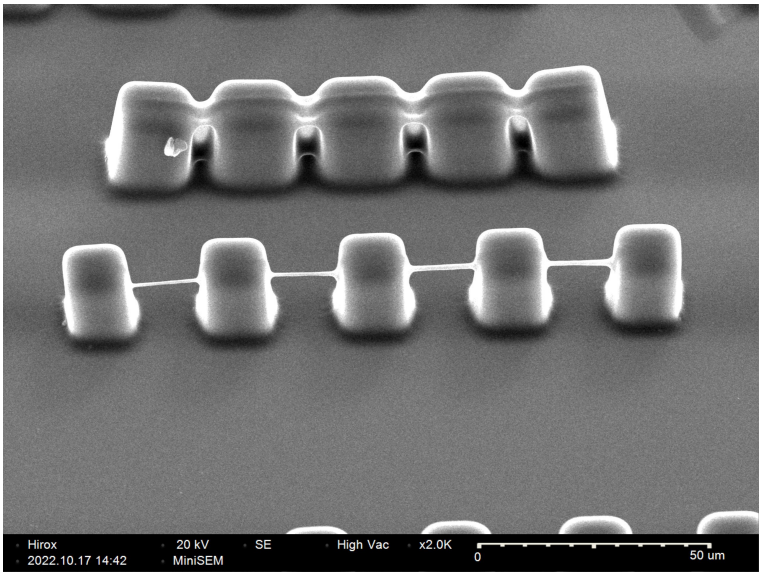

Figure 8: Fully 3D structures

Based on our simulations, we were able to progress to fabricate fully 3D structures, as shown in Figure 8. To obtain these structures, we exposed different SLM patterns in two different focus planes. The first exposure was focused on the substrate level to fabricate blocks, the image displayed on the SLM at this focus consists of five white squares of 21.25 µm side on a black background. The image for the second exposure is a thin line of 2.1 µm wide focused 14 µm above the initial focus plane. Figure 8 indicates that it is possible to obtain micron level resolution with our TTA resist. Our current difficulties center on obtaining this resolution reproducibly. These digital models and simulations are an important tool in improving reproducibility.

4 Conclusion

We have successfully developed a phenomenological digital model of the photo-chemical process for the parallelized multiphoton fabrication of 3D structures by imaging an amplitude SLM into a TTA resist. In our model, 3D optical propagation and chemical diffusion are performed. The simulation currently gives reasonable predictions of 2D and 2.5D structures (single exposure) and has helped us improve 3D structures resolution (2 exposures). Our current work centers on improving the model (calibration and obtaining a Modulation Transfer Function (MTF) description of our system) and parallelizing simulations to enable us to model larger structures.

Acknowledgements

IMT Atlantique and ENS Lyon authors acknowledge support from the Agence Nationale de la Recherche ANR for the grant "New 3D print". IMT Atlantique and ICube authors acknowledge the IMT Carnot research program for doctoral funding for author F.O. . This work has received funding from the European Union's Horizon 2020 and Horizon Europe research and innovation programs under grant agreements N^{o}780278 and N°101091644. The dissemination of results herein reflects only the author's view and the

European Commission is not responsible for any use that may be made of the information it contains. All authors thank Patrice Baldeck from ENS Lyon for many helpful discussions.

References

[1] T. Bladacchini, Three-dimensional microfabrication using two-photon polymerization, Elsevier, Waltham, MA, USA **2016**;

[2] D. Gonzalez-Hernandez, S. Varapnickas, A. Bertoncini, C. Liberale, M. Malinauskas, *Adv. Opt. Mater.* **2023**, 11, 2201701;

[3] M. Farsari, B. N. Chichkov, *Nat. Photonics* **2009**, 3, 450;

[4] S. Thiele, K. Arzenbacher, T. Gissibl,H. Giessen, AM. Herkommer, *Sci. Adv.* **2017**, 3, e1602655;

[5] J. Li,P. Fejes,D. Lorenser,B.C. Quirk,P.J. Noble,R.W. Kirk, A. Orth, F.M. Wood, B. C. Gibson, D.D. Sampson, R.A. McLaughlin, *Sci. Rep.* **2018**, 8,14789;

[6] B. Spagnolo, V. Brunetti, G. Leménager, E. De Luca, L. Sileo, T. Pellegrino, P.P. Pompa, M. De Vittorio, F. Pisanello,*Sci. Rep.* **2015**,5,10531;

[7] E.D. Lemma, S. Sergio, B. Spagnolo, M. Pisanello, L. Algieri, M.A. Coluccia, M. Maffia, M. De Vittorio, F. Pisanello, *Microelectron. Eng.* **2018**,190,11;

[8] J. Maciulaitis, M. Deveikytė, S. Rekštytė,M. Bratchikov,A. Darinskas,A. Šimbelytė, G. Daunoras, A. Laurinavičienė, A. Laurinavičius, R. Gudas, M. Malinauskas, R. Mačiulaitis, *biofabrication* **2015**, 7,015015;

[9] C. Arnoux, L.A. Pérez-Covarrubias, A. Khaldi, Q. Carlier, P.L. Baldeck, K. Heggarty, A. Banyasz, C. Monnereau, *Addit. Manuf.* **2022**, 49, 102491;

[10] C. Maibohm, O.F. Silvestre, J. Borme, M. Sinou, K. Heggarty, J.B. Nieder, *Sci. Rep.* **2020**, 10, 8740;

[11] E. Skliutas, M. Lebedevaite, E. Kabouraki, T. Baldacchini, J. Ostrauskaite, M. Vamvakaki, M. Farsari, S. Juodkazis, M. Malinauskas, *Nanophotonics* **2021**, 10, 1211;

[12] J. Kato, N. Takeyasu, Y. Adachi, H.B. Sun, S. Kawata *Appli. Phys. Lett.* **2005**, 86, 044102;

[13] M.V. Kessels, M. El Bouz, R. Pagan, K. Heggarty, *J. Micro/Nanolithogr., MEMS, MOEMS* **2007**, 6, 033002;

[14] Heidelberg Instruments, https://heidelberg-instruments.com/legal-notice/, accessed : June, **2023**;

[15] V. Hahn,N.M. Bojanowski,P. Rietz,F. Feist,M. Kozlowska, W. Wenzel,E. Blasco, S. Bräse, C. Barner-Kowollik, M. Wegener, *ACS Photonics* **2023**, 10,24;

[16] Z. Wang, Y. Zhang, Y. Su,C. Zhang, C. Wang, *Sci. China: Chem.* **2022**,65,2283;

[17] S.N. Sanders,T.H. Schloemer,M.K. Gangishetty,D. Anderson,M. Seitz, A.O. Gallegos, R.C. Stokesb, D.N. Congreve, *Nature* **2022**, 604,474;

[18] D.K. Limberg, J. Kang, R.C. Hayward, *J. Am. Chem. Soc.* **2022**, 12, 5226;

[19] P. Baldeck, A. Banyasz, WO2019025717A1, https://patents.google.com/patent/WO2019025717A1/fr, **2019**;

[20] E. Papagiakoumou, E. Ronzitti, V. Emiliani, *Nat. Methods* **2020**, 17, 571;

[21] V.Hahn,P. Rietz,F. Hermann,P. Müller,C. Barner-Kowollik, T. Schlöder, W. Wenzel, E. Blasco, M. Wegener, *Nature Photonics* **2022**, 16,784;

[22] D. Voelz, Computational Fourier Optics, SPIE Press, Bellingham, Washington, USA 2011;

[23] J. Wen, Y. Zhang, M. Xiao, *Adv. Opt. Photonics* **2013**, 5,83;

[24] M. Abramowitz,K.R Spring, H.E. Keller, MW. Davidson *Bioimaging* **2002**,33,772;

[25] A. Erdmann, Optical and EUV Lithography, SPIE, Bellingham, WA, USA **2021**;

[26] H. Kirshner, F. Aguet, D. Sage, M. Unser, *J. Microsc* **2013**, 249,13;

[27] A. Kalpattu, T. Dilbeck,K. Hanson, J.T. Fourkas *Phys. Chem. Chem. Phys.* **2022**, 24,28174;

[28] D.A. Bernard *IEEE Trans. Semicond. Manuf.* **1988**, 1,85.